

Comparison of blended versus layered structures for poly(*p*-phenylene vinylene)-based polymer photovoltaics

S. V. Chasteen^{a),b)} and J. O. Härter

Physics Department, ISB, University of California-Santa Cruz, Santa Cruz, California 95064

G. Rumbles

National Renewable Energy Laboratory, Center for Basic Science, MS 3216, 1617 Cole Boulevard, Golden, Colorado 80401

J. C. Scott

IBM Almaden Research Center, 650 Harry Road, San Jose, California 95120

Y. Nakazawa

Physics Department, ISB, University of California-Santa Cruz, Santa Cruz, California 95064

M. Jones

National Renewable Energy Laboratory, Center for Basic Science, MS 3216, 1617 Cole Boulevard, Golden, Colorado 80401

H.-H. Hörhold and H. Tillman

Institut Für Organische Chemie und Makromolekulare, University of Jena, Humboldtstrasse 10, Germany

S. A. Carter^{a),c)}

Physics Department, ISB, University of California-Santa Cruz, Santa Cruz, California 95064

(Received 5 August 2005; accepted 14 December 2005; published online 14 February 2006)

We characterize and compare blended and bilayered heterojunctions of polymer photovoltaic devices using poly[oxa-1,4-phenylene-1,2-(1-cyano)-ethenylene-2,5-dioctyloxy-1,4-phenylene-1,2-(2-cyano)-ethenylene-1,4-phenylene] (CN-ether-PPV) and poly[2,5-dimethoxy-1,4-phenylene-1,2-ethenylene-2-methoxy-5-(2-ethylhexyloxy)-1,4-phenylene-1,2-ethenylene] (M3EH-PPV) as electron- and hole-transporting polymers, respectively. We find that both blended and bilayered structures have substantially improved current densities (>3 mA/cm²) and power efficiencies ($\sim 1\%$ under white light) over neat films. Improved exciton dissociation at multiple interfaces and reduced recombination due to energy and charge transfers increases the charge-carrier collection in both types of heterojunction devices, but low electron mobilities in the polymers lead to low fill factors and reduced quantum efficiency ($\sim 20\%$) that limit the power efficiency. Time-resolved photoluminescence reveals that for blended structures both the hole and electron-transporting polymers undergo efficient quenching with the exciton decay being dominated by the existence of two fast decay channels of 0.12 and 0.78 ns that are assigned to interspecies charge transfer and account for the increased short-circuit current observed. For layers, these components are not as prevalent. This result indicates that greater exciton generation at the dissociating interface and more efficient charge collection in the thin layers is primarily responsible for the improved short-circuit current, a conclusion that is further supported by numerical simulations of the exciton generation rate and charge collection. We also report evidence for an intermediate exciplex state in both types of structures with the greatest yield for blends with 50 wt % of CN-ether-PPV. Overall, the improved performance is due to different processes in the two structures; efficient bulk exciton quenching and charge transfer in blends and enhanced exciton generation and charge collection in layers. The optimization of each photovoltaic heterostructured device relies on this understanding of the mechanisms by which each material architecture achieves high power efficiencies. © 2006 American Institute of Physics. [DOI: [10.1063/1.2168046](https://doi.org/10.1063/1.2168046)]

I. INTRODUCTION

Polymer photovoltaics have attracted a lot of attention in recent years because they offer a pathway for producing inexpensive electricity from the sun due to the inherent low cost of polymer processing. Still, after a decade of research,

the device efficiency of polymer photovoltaics lags behind that of the inorganics by nearly an order of magnitude. The performance of these organic devices is severely limited by poor exciton dissociation and charge transport due in part to high rates of exciton recombination and low charge mobilities in polymers. Polymer film thicknesses on the order of the length scale for exciton recombination are required for efficient charge collection; however, such thin films normally suffer from poor absorption. This tradeoff can be partially

^{a)}Authors to whom correspondence should be addressed.

^{b)}Electronic mail: stephanie@physics.ucsc.edu

^{c)}Electronic mail: sacarter@cats.ucsc.edu

overcome through the use of blended and layered heterojunctions. Such morphologies offer multiple exciton dissociation sites and separate charge pathways, thus limiting exciton recombination, and allowing for thicker, more absorbing, polymer films.

Blends of electron-acceptor and -donor materials result in dramatically enhanced device performances and high degrees of photoluminescence quenching relative to their neat film counterparts,^{1–5} due in part to multiple, closely spaced, dissociation interfaces and separate charge pathways for the electrons and holes; however, control over domain size and morphology in such films is difficult. Less attention has been afforded to bilayered polymer devices where the large interfacial area between the donor and acceptor provides an additional interface for exciton dissociation, with charge transport expected to be improved over blends due to the potential for more ordered, shorter charge-transport pathways and less probability for bimolecular recombination. In addition, layer thickness is easier to control than domain size although material choice is more limited since the first layer cannot be dissolved in the process of spin coating the second. Polymer/polymer bilayers [such as PPV/BBL,⁶/MEH-CN-PPV/POPT,⁷ and PPyV/PAT6 (Ref. 8)], polymer/C₆₀,^{9,10} and polymer/small molecule^{11,12} have shown improved device performance over comparable single-layer films.

A comparison of blended and layered MEH-PPV:C₆₀ devices found higher currents in the blended device,¹⁰ but PPV:C₆₀ blended cells were found to have poorer charge transport than similar layered devices.¹³ Due to the inability to tune the absorption of C₆₀ and difficulties in controlling the blend morphology and C₆₀ solubility in different polymer films, some effort has been taken to replace the C₆₀ with either another nanoparticle or with an electron-transporting polymer. For these systems, no direct comparison between blends and layers of electron- and hole-transporting materials has been undertaken. In this paper, we compare electron- and hole-transporting polymers in blended and layered film morphologies in order to better understand charge generation and transport in these materials. Our results suggest a pathway for optimizing the polymer film morphology to achieve greater power efficiency for polymer-based photovoltaics.

II. METHODS

We chose poly[2,5-dimethoxy-1,4-phenylene-1,2-ethynylene-2-methoxy-5-(2-ethylhexyloxy)-1,4-phenylene-1,2-ethynylene] (M3EH-PPV) as our hole transporting polymer and poly[oxa-1,4-phenylene-1,2-(1-cyano)-ethynylene-2,5-dioctyloxy-1,4-phenylene-1,2-(2-cyano)-ethynylene-1,4-phenylene] (CN-ether-PPV),¹⁴ as our electron transporter. M3EH-PPV, shown in Fig. 1, is an alternating copolymer of the well-characterized semiconducting polymer poly[2-methoxy-5-(2'-ethylhexyloxy)-1,4-phenylene-vinylene] or MEH-PPV. M3EH-PPV was synthesized by Horner reaction and has optical properties very similar to MEH-PPV;¹⁵ however, due to the limited length of the side chains, M3EH-PPV is much less soluble than MEH-PPV and enables multilayered structures as well as a greater hole mobility. As a hole acceptor and hole transporter, it has a hole mobility on the

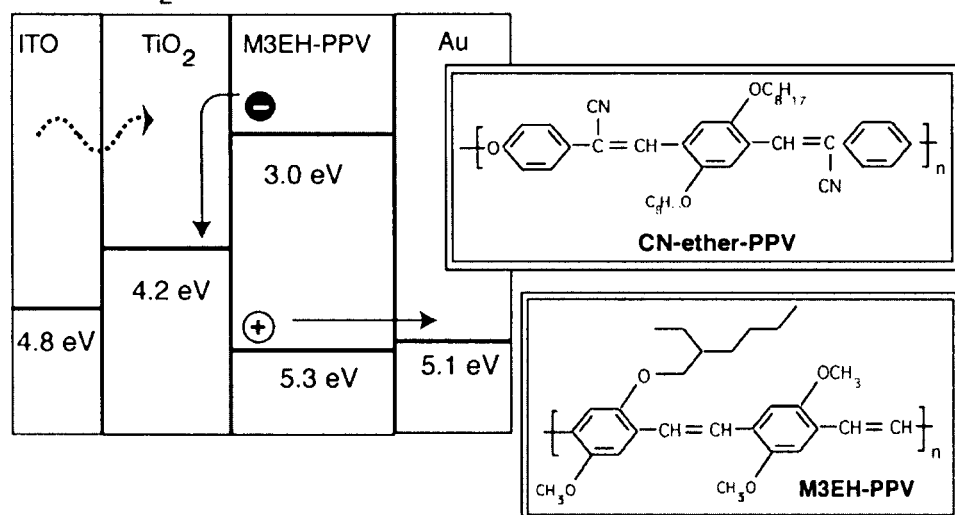
order of 10⁻⁵ cm²/Vs at 300 K and under moderate electric fields. It has highest occupied molecular orbital (HOMO) and lowest unoccupied molecular orbital (LUMO) levels of 5.3 and 3.0 eV, respectively.

CN-ether-PPV, shown in Fig. 1, is a derivative of the relatively insoluble polyconjugated poly(2,5,2',5'-tetrahexyloxy-8,7'-dicyano-di-*p*-phenylene vinylene) or CN-PPV and is designed to increase solubility and electron affinity relative to CN-PPV. It is nearly identical in structure to the conjugated polymer PCNEPV, used by another group.^{16,17} It has HOMO and LUMO levels of 5.9 and 3.5 eV, respectively. MEH-PPV and CN-PPV phase separate on the order of the exciton diffusion length of 20 nm,⁵ and poly[2-methoxy-5-(3,7-dimethyloctyloxy)-1,4-phenylenevinylene] (MDMO-PPV) and PCNEPV phase separate on the order of 30–50 nm,^{16,17} and have been used in blended devices with good results,^{4,5,16} and we expect the same to be true in our system. The selective solubility of M3EH-PPV, which dissolves well in chlorobenzene but poorly in both toluene and *p*-xylene, allows us to spin-cast layered devices. Thus, CN-ether-PPV in *p*-xylene spin cast on top of M3EH-PPV in chlorobenzene should result in layers with relatively low blending of the polymers at the interface.

The heterojunction photovoltaic devices were prepared using two different electrode structures with opposite charge-transport polarity. The transparent electron-accepting structure ITO/TiO₂/polymer/Au [Fig. 1(a)] forces the holes to travel the bulk of the polymer layer, and the transparent hole-accepting structure ITO/PEDOT-PSS/polymer/Al [Fig. 1(b)] forces the electrons to travel across the bulk. Neat M3EH-PPV devices and blends of M3EH-PPV:CN-ether-PPV may be fabricated on either structure; however, layered devices are restricted to the PEDOT/M3EH-PPV/CN-ether-PPV/Al structure because of the high solubility of CN-ether-PPV. We note that we were unsuccessful in making photovoltaics with appreciable open-circuit voltage from neat CN-ether-PPV films, presumably due to high leakage, poor mobility, or dewetting of CN-ether-PPV from the substrate.^{17,18}

Devices are prepared and characterized as described elsewhere.¹⁹ TiO₂ is made from a sol-gel precursor solution.²⁰ A transparent semiconductor TiO₂ acts as an electron transporter and hole blocker due to its energy-level structure [Fig. 1(a)]. When light is incident on TiO₂, it becomes relatively conducting such that the quasi Fermi-level of the photodoped TiO₂ appears to play an important role in determining the open-circuit voltage. PEDOT-PSS from Bayer is a metallic polymer that acts as an oxygen barrier and planarizing layer and has a substantially lower work function (~5.1 eV) than ITO (~4.8 eV), leading to greater open-circuit voltage. Both TiO₂ and PEDOT-PSS have been shown to improve device performance over bare ITO.^{21,22}

Steady-state and time-resolved photoluminescence measurements were performed at the National Renewable Energy Laboratory. Steady-state photoluminescence spectra were recorded using a Fluorolog-3 (JYHoriba) spectrometer that utilized a liquid-nitrogen-cooled charge-coupled device (CCD) detector. Monochromatic excitation light was generated by a xenon arc lamp with double monochromator. Fluorescence was collected at 90° relative to the excitation beam,

(a) ITO/TiO₂/polymer/Au

(b) ITO/PEDOT/polymer/Al

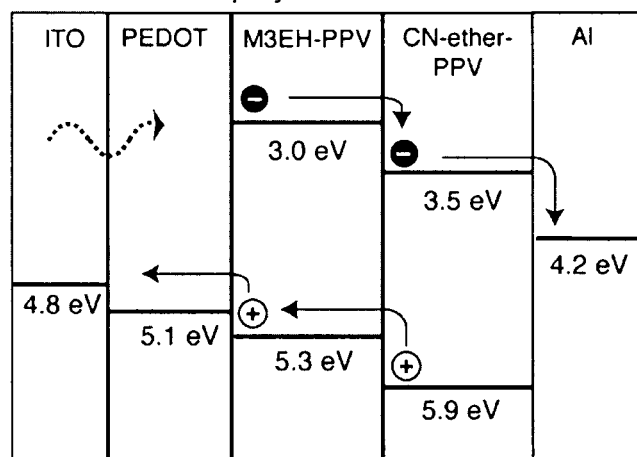


FIG. 1. Energy-level diagrams for different device structures, plus chemical structure of polymers (inset). The PEDOT||Al structure forces holes to cross the bulk from the first incident electrode, whereas the TiO₂||Au structure forces the electrons to cross the bulk.

passed through a single monochromator containing a 300 line/mm grating, and imaged on the liquid-nitrogen-cooled CCD array. All photoluminescence (PL) spectra were corrected for the spectral output of the excitation source and for the spectral response of the detection optics.

Fluorescence decay signals were measured using the technique of time correlated single-photon counting (TCSPC).²³ The spectrometer comprised a pulsed, picosecond diode laser (IBH NanoLED-10) operating at a wavelength of 438 nm and a repetition rate of 1 MHz. Emission was detected at 90° to excitation by focusing the emission onto the slits of a 0.25 m monochromator (SPEX minimate) and subsequently detected by a photon counting photomultiplier tube (Hamamatsu H6279). The instrument response function (IRF) from this system when scattering the excitation light from a dilute solution of colloidal silica was determined to be 220 ps. Using a nonlinear, least-squares iterative deconvolution procedure employing the Marquardt minimization routine, the influence of the IRF could be removed from the measured luminescence decay curves to reproduce the true decay kinetics with a temporal resolution of ~30 ps.

Current-density versus voltage curves were measured using a 2400 Keithley source meter. Due to the electric-field reversal across device architectures, ITO was sourced nega-

tive in TiO₂||Au devices and positive in PEDOT||Al devices, resulting in *J-V* curves located in quadrant IV. The voltage is sourced from -1.0 to 1.0 V in 0.02 V steps. Illumination is provided by a white light bulb with an output of approximately 80 mW/cm².

Photoaction current spectra are taken with the same 2400 Keithley source meter. Illumination is provided by a 150 W Oriel xenon arc lamp, whose output is focused upon the substrate by use of a liquid light guide. The wavelength of incident light is controlled with an Oriel Corner Stone 130 1/8 m motorized monochromator, and incremented from 350–700 nm in 10 nm steps with a 150 ms pause at each wavelength. External quantum efficiency is measured by normalizing that current output by the current and external quantum efficiency of a silicon photodetector mounted in the testing apparatus. Absorption spectra are taken on a Varian optical spectrometer.

III. RESULTS

A. Device characterization

1. *J-V* curves and external quantum efficiency

In Fig. 2 we show typical current-voltage (*J-V*) curves for optimized devices. Blended and layered devices that are

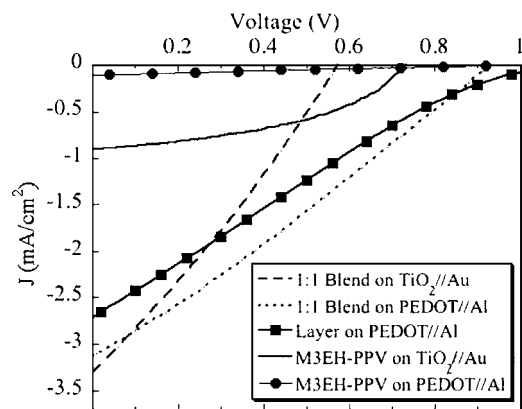


FIG. 2. J - V Curves for optimized devices showing how the open-circuit voltage, current, and fill factor varies with device architecture. Blended devices perform equally well on both device polarities, indicating bipolar charge transport; the same is not true of M3EH-PPV. The blended and layered structures show similar performance. ITO is sourced negative in $\text{TiO}_2//\text{Au}$ devices, for ease of comparison across architectures. The device thicknesses are 40 ± 10 nm, except for the layered device, which is 25 nm M3EH-PPV/50 nm CN-ether-PPV.

optimized for performance show similar short-circuit current densities, up to 3.3 mA/cm^2 at 80 mW/cm^2 white light intensity, more than a threefold improvement over neat M3EH-PPV films on TiO_2 and 13-fold over M3EH-PPV on PEDOT. We observed more variations in device performance for layered structures and current densities were higher, on average for blends than for layers. Film thicknesses for optimized devices were normally 30 ± 5 nm for each polymer layer, except for layers in which the best device had thicknesses of 20 nm M3EH-PPV/50 nm CN-ether-PPV. Peak power conversion efficiency was 0.35% for plain M3EH-PPV on TiO_2 and ranged from 0.66% to 1% for blended and layered devices, the variability being due to changes in V_{oc} across device structures. In blends, V_{oc} was adversely affected by an increase in the percent of CN-ether-PPV in the blend, suggesting large leakage in that polymer. Transport in CN-ether-PPV is likely to be disrupted by the presence of ether groups, which disrupt the conjugation and thus intrachain transport. V_{oc} was higher in layers than in blends, indicating that V_{oc} is created by the HOMO/LUMO difference in layers, but by V_{bi} due to the electrodes in blends, a conclusion supported by simulations not reported here.²⁴

Maximum external quantum efficiency was 24% for blends, 15% for layers, and 7% for neat M3EH-PPV films. The external quantum efficiency of blended and layered devices was mostly symbatic with the absorption curves of the neat films, indicating efficient charge separation throughout the bulk. This evidence points towards the electrode/M3EH-PPV and the M3EH-PPV/CN-ether-PPV interfaces as being the important areas for exciton dissociation, rather than the CN-ether-PPV/electrode interface, though there is some variability in quantum efficiency curves indicating variability in film morphology across devices. Blended and layered devices with similar short-circuit currents had similar peak quantum efficiencies.

The dramatic improvement of device performance of blended and layered devices ($J \sim 3.3 \text{ mA/cm}^2$) over neat M3EH-PPV ($J = 0.07 \text{ mA/cm}^2$) films on PEDOT//Al is a

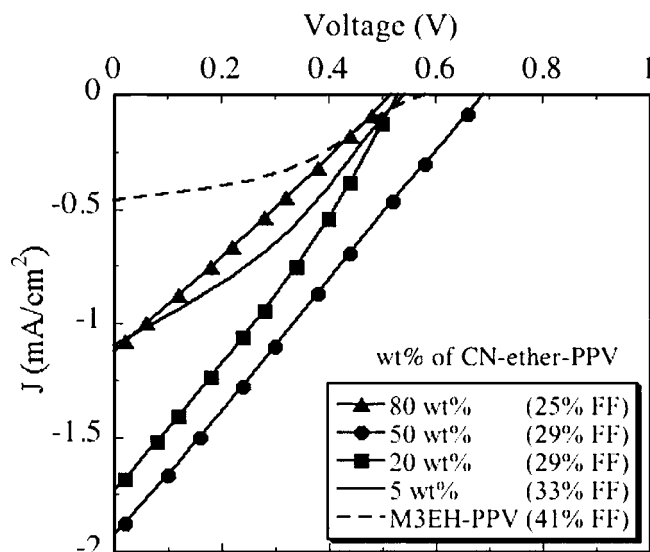


FIG. 3. J - V Curves for various blend ratios showing the increase in short-circuit current for blends over neat films. Optimal current occurs for 50 wt% blends. The fill factor is reduced as CN-ether-PPV concentration increases. All devices are on $\text{TiO}_2//\text{Au}$ structure and are 55 ± 15 nm thick. Wt % is given in wt % of CN-ether-PPV in the blend.

strong indication of more efficient exciton dissociation and charge collection. Neat M3EH-PPV devices on $\text{TiO}_2//\text{Au}$ have current densities ($J = 0.9 \text{ mA/cm}^2$) more than 13 times higher than those for M3EH-PPV on PEDOT//Al ($J = 0.07 \text{ mA/cm}^2$), due to the poor electron mobility of M3EH-PPV and the use of a transparent electron-accepting structure that forces the poorly mobile electrons to travel the bulk.²⁰ Unlike these single-layer M3EH-PPV devices, blended devices performed equally well on both the $\text{TiO}_2//\text{Au}$ and PEDOT//Al structures. Thus device polarity is no longer a limiting factor in these bulk heterojunction devices and both charge carriers are able to exit the device. When device polarity of layered devices was reversed by deposition of the CN-ether-PPV layer prior to the M3EH-PPV layer (resulting in a partially but not totally blended device), V_{oc} and I_{sc} reversed direction, because the internal electric field is created by the HOMO/LUMO offset of the polymers. This is consistent with the assumption that holes exit the device through M3EH-PPV and electrons through the CN-ether-PPV, following separate charge pathways thus minimizing recombination.

We tested a variety of blend ratios from 5 to 90 wt% CN-ether-PPV in M3EH-PPV:CN-ether-PPV blends (see Fig. 3). Blends with 50 wt% CN-ether-PPV exhibited the highest currents and power efficiencies. Other groups examining related MEH-PPV:CN-PPV blends have used a variety of blend ratios and found the most efficient quenching with 21–29 wt%, indicative of a difference in the relative charge-carrier mobilities in the two systems. The fill factor plummeted as we increased the percent of CN-ether-PPV in the blend, with typical values above 40% for $\text{TiO}_2//\text{M3EH-PPV}/\text{Au}$ and 30% for blends on $\text{TiO}_2//\text{Au}$ (25% on PEDOT//Al). Layered devices were also compromised by these low fill factors, around 25%. The decrease in fill factor is consistent with other recent studies,^{16,18} and suggests relatively poor electron transport in the CN-ether-PPV.

All blended devices were transport limited, not absorption limited. Current density decreased as the thickness of the device was increased, for neat M3EH-PPV devices and 50 wt % blends with CN-ether-PPV. The current of blended devices fell by nearly a factor of 2 from a 30- to a 90-nm-thick film. This is similar to findings for neat-film devices where the drop is more appreciable.^{19,20} Poor charge transport is due in part to the poor electron transport in CN-ether-PPV, charge hopping from domain to domain in phase-separated blends, and domain sizes that may be larger than the exciton diffusion length in M3EH-PPV (<10 nm).

For layered devices, the relationship between device performance and layer thickness was less clear (see Fig. 7). The best device was comprised of 25 nm M3EH-PPV/50 nm CN-ether-PPV layers, slightly thicker than equal layer thicknesses of 30 nm which also gave good results. In general, device performance varied inversely with M3EH-PPV thickness. Similar data were observed for PPV/BBL bilayer devices, where layers of 50 nm each gave the best device performance.⁶ To understand the changes that occur in our layered devices with thickness, we had to consider how optical interference and absorption affected the exciton generation rate (Fig. 9). These simulations are discussed in Sec. III B.

The increased current density for layered heterojunction devices is caused in part by greater exciton dissociation due to increased interfacial area. However, since the layer structure can only account for at most a doubling or tripling of the interfacial area available for charge dissociation, the enhanced interfacial area cannot account for the 13-fold current increase of a layered device over neat M3EH-PPV film, as shown in Fig. 2. Thus, the current increase is attributable to increased charge collection in thinner polymer layers and reduced charge recombination due to separate charge pathways and subsequent greater efficiency of charge collection.

An unexpected result of our device measurements was the similarity in the performance of optimized blended and layered devices (although on average blends outperformed layers) despite drastically different morphology. Nonetheless, time-resolved measurements and device simulations suggest that different mechanisms are responsible for device performance enhancement. The similarity could suggest some interpenetration of the layers at the polymer/polymer interface in layered devices, resulting in a somewhat blended device. The total device thickness was consistently ~ 10 nm thinner compared to the combined thicknesses of each polymer layer spun alone, suggesting about 10 nm of commingling at the interface. Spectroscopy data, discussed in Sec. III A 2 below, suggest that the recombination pathways in the 30 nm M3EH-PPV/30 nm CN-ether-PPV layered device are very different than 50 wt % blended devices, though similar to a 86 wt % blend device. Thus, if there is blending at the interface, it is incomplete.

2. Absorption and steady-state photoluminescence

Relative absorption and photoluminescence spectra for blended films are shown in Fig. 4, and for layered films in Fig. 5. In both blended and layered films, the absorption curve closely matched a linear combination of the composite

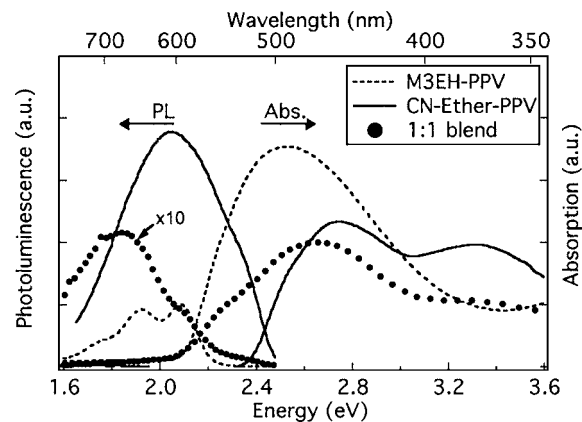


FIG. 4. Relative photoluminescence and absorption for M3EH-PPV, CN-ether-PPV, and blended films on quartz substrates. The higher-energy states in the neat films are highly quenched in the heterostructures, leaving exciplex emission at 1.8 eV. All films are 100 ± 15 nm thick. Relative photoluminescence data was excited at 2.82 eV (600 nm) and was corrected for optical density of the film. Relative photoluminescence data have a 20% margin of error in data reproducibility.

polymers, with roughly equal weight. This result implies (a) that the polymers are not interacting in the ground state (e.g., to form additional aggregate species) and (b) that equal weight fractions correspond roughly to equal volume fractions in film. Because we observe a factor of 2 greater absorption coefficient in M3EH-PPV compared to CN-ether-PPV, appreciably greater exciton generation is expected to occur in M3EH-PPV for similar film thickness.

Relative photoluminescence measurements revealed that both blends and layers were strongly quenched relative to the neat films. The 20 nm/20 nm layers were quenched by 87% relative to 20 nm CN-ether-PPV, and a blend comprised of 50 wt % CN-ether-PPV was quenched by 94% relative to CN-ether-PPV of the same thickness, indicating more efficient exciton dissociation and reduced recombination in heterojunctions as expected. The photoluminescence peak of

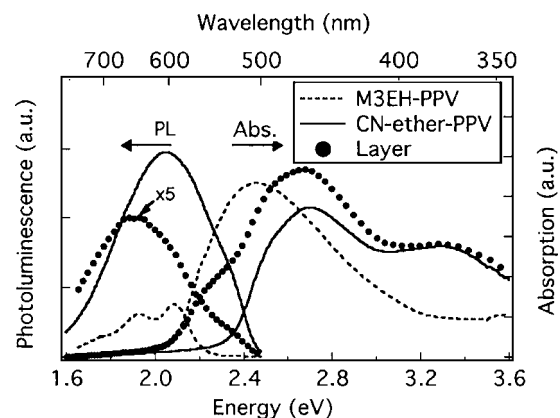


FIG. 5. Relative photoluminescence and absorption for M3EH-PPV, CN-ether-PPV, and layered films on quartz substrates, showing quenching in the layered film. The layered film is less quenched than the blended film, and only a slight shift towards an exciplex peak at 1.8 eV is observed. All films are 20 ± 5 nm thick. Layered sample consists of 20 ± 5 -nm-thick layers. Relative photoluminescence data were excited at 2.82 eV (600 nm) and were corrected for optical density of the film. PL data have a 20% margin of error in data reproducibility. Layered device absorption is a 1+1 linear combination of M3EH-PPV and CN-ether-PPV absorption.

highly luminescent CN-ether-PPV is strongly quenched in the steady state. Some of this quenching in the 2.1–2.4 eV range could be due to Foerster energy transfer from CN-ether-PPV to M3EH-PPV since considerable overlap occurs between the photoluminescence spectrum of CN-ether-PPV and the absorption spectrum of M3EH-PPV in that region. The photoluminescence of heterojunction films peaks at about 1.9 eV in layers and 1.8 eV in blends. The spectra for blends or for layers differ significantly from a linear combination of neat films, even considering a higher weight of M3EH-PPV emission than expected due to Foerster transfer. We take the new 1.8 eV peak in blends and the PL shift in layers to be indicative of a charge-transfer state between an electron on CN-ether-PPV and a hole on M3EH-PPV (an energy gap of 1.8 eV), i.e., an exciplex. Exciplexes have been reported only a few times previously in π -conjugated polymers,^{25–28} including a recent study of MDMO-PPV:CN-ether-PPV blends which reported an exciplex peak at 1.85 eV.²⁸ The existence of an exciplex or similar charge-transfer state in both types of heterostructures is supported by the fact that neither layers nor 50 wt % blends exhibit the characteristic photoluminescence of M3EH-PPV when excited at 2.3 eV, where only M3EH-PPV absorbs. Instead, the peak at 1.8 eV remains or shifts, while a small shoulder due to M3EH-PPV emission grows. Thus, at the least, charge transfer occurs from M3EH-PPV to CN-ether-PPV. The exciplex peak intensity increases with increased wt % of CN-ether-PPV in the blend, suggesting that charge transfer also occurs from CN-ether-PPV to M3EH-PPV, as observed in MDMO-PPV:CN-ether-PPV blends within 100 ps after excitation.²⁸ The presence of neat-film photoluminescence indicates that radiative recombination also takes place within each polymer as well as within the exciplex.

3. Time-resolved photoluminescence

To obtain a better understanding of how the different film morphologies are affecting the excited-state dynamics, time-resolved photoluminescence decays were measured for films on quartz (no electrodes). Decays were fit to exponential decay functions. While previous groups have found equally good fits for stretched exponentials in MEH-PPV (Ref. 29), the repeatability of decay components across samples and heterojunctions is a convincing evidence that the measured decays are intrinsic features of these films. It is important to note that the measured decay times may not represent carrier lifetimes; two or more interconverting species (such as intrachain excitons, excimers, or exciplexes) will show equal decay times represented by a quadratic function of the two decay times.³⁰ Average decay time was calculated as the lifetime weighted by the yield for each exponential. Results are given in Fig. 6 and Table I. Decays were force fit to double and triple exponentials for neat films and heterojunctions, respectively. Attempts to fit to fewer parameters resulted in poor fits, as demonstrated by the fact that the reduced χ^2 at least doubled; all reported fits have reduced χ^2 of 1.0 or 1.1 and Durbin-Watson of 1.7 or greater.²³ This number of exponentials indicates the presence of multiple exciton decay mechanisms as could be expected from thin polymer films where interchain and intrachain dynamics, as

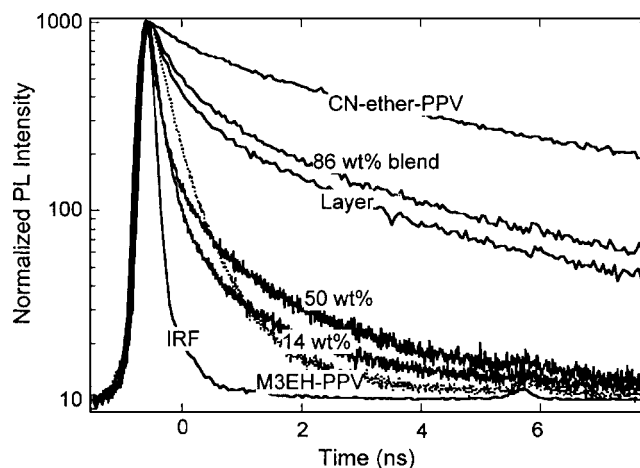


FIG. 6. Decay curves for pristine polymers, blends with 14, 50, and 86 wt % CN-ether-PPV, and 30 nm/30 nm M3EH-PPV/CN-ether-PPV layers at 600 nm emission. All films are 30 nm thick. Decay is more rapid with increasing percentage of M3EH-PPV in the blend, especially at short time scales. Layered films have longer decays despite similar current as the 50 wt % blend. Decay for 86 wt % blends is more rapid than that for 50 wt % blends, despite superior performance in the latter. The layered film is illuminated through the quartz substrate, exciting the M3EH-PPV layer first as in actual device structure. Decays for thicker films (not shown) are longer. Intensity is normalized to 1000 counts with a background of 10.

well as charge transfer, can all lead to distinct decay species. Energy transfer (i.e., Foerster transfer) should not play a significant role at 2.06 eV due to the low absorption of M3EH-PPV at that energy.

The decay of M3EH-PPV was dominated by a fast component of 0.30 ns (92% yield), which suggests the presence of an intrachain exciton due to its fast decay, but we do not assign specific components to inter- or intrachain excitations, in keeping with previous work,³¹ due to the inherent error involved in such assignments. The decay of M3EH-PPV was very similar to that previously reported for MEH-PPV,^{28,29} though slightly faster, and steady-state luminescence was measured to be less than half that of MEH-PPV. This indicates the presence of highly efficient nonradiative recombination paths in M3EH-PPV. We estimate the quantum yield and natural lifetime of M3EH-PPV by integrating the relative steady-state photoluminescence of M3EH-PPV and MEH-PPV and using the relative magnitudes as a correction factor for the quantum yield of MEH-PPV films (0.12).³² Taking into account the experimental error in relative steady-state

TABLE I. Excited-state lifetime. Reduced χ^2 is 1.0 or 1.1 for all samples except the 14 wt % blend with a χ^2 of 1.2. Percent yield is reported in parentheses after each decay component. Blend wt % is given with respect to wt % of CN-ether-PPV in the blend. Emission wavelength is 600 nm. Layered devices are illuminated through the M3EH-PPV.

Film	τ_1 (ns)	τ_2 (ns)	τ_3 (ns)	Ave. τ (ns)
M3EH-PPV	0.30(92%)	1.4 (8%)		0.38 ns
CN-ether-PPV	11.0 (66%)	3.5 (33%)		8.5 ns
14 wt % blend	0.12(67%)	0.78(20%)	3.5 (12%)	0.67 ns
50 wt % blend	0.12(59%)	0.78(24%)	3.5 (18%)	0.87 ns
86 wt % blend	3.5 (42%)	11.0 (38%)	0.78(21%)	5.7 ns
30 nm/30 nm layer	3.5 (42%)	11.0 (40%)	0.78(19%)	5.9 ns

photoluminescence measurements, we estimate a quantum yield of 0.03–0.07 and a natural radiative lifetime of 5.4–12.7 ns.

The decay of CN-ether-PPV was dominated by a long component of 11.0 ns (66%), which we take to be the inter-chain exciton, or excimer, and a secondary component of 3.5 ns (33%), which we take to be the intrachain exciton. We base this assumption upon arguments from previous studies of temperature dependence and photoluminescence in film and solution of CN-PPV,³³ the broad redshifted steady-state spectrum, and the longer decay in film as compared to solution, indicating a species that is weakly coupled to the ground state.

Quenching of the excited state is readily observed in both the blended and layered heterojunction devices (see Fig. 6 and Table I), where the decay times were significantly reduced with respect to the pristine polymers. A fast 0.05–0.12 ns component dominates the decay at 650 nm (the emission peak of the pristine polymers) for most of the blends and for some layered films. We consider this to be the 0.30 ns M3EH-PPV component shortened due to charge and energy transfers to CN-ether-PPV or the exciplex. This conclusion is supported by the increased yield of this component for blends with higher wt % of M3EH-PPV in the blend. This fast component indicates that the charge transfer from excitons in M3EH-PPV competes efficiently with radiative and nonradiative recombinations in these films and accounts for the increased current in blends. The substantially lower weight and longer decay time of this fast component compared to the blends of M3EH-PPV with phenyl-*C*₆₁-butyric acid methyl ester (PCBM) would imply that either CN-ether-PPV:M3EH-PPV blends form larger domains than M3EH-PPV (limiting exciton dissociation) or that CN-ether-PPV is not as good as an electron acceptor as PCBM. In either case, the short-circuit current would be lower for the polymer:polymer blend than for polymer:*C*₆₀, as observed experimentally. Blends of M3EH-PPV with 80 wt % PCBM exhibit short-circuit currents about two to three times as high as blends with 50 wt % CN-ether-PPV.

Of particular interest is the presence of a new decay component of 0.78–2.0 ns in all heterojunction structures, with a yield of roughly 20% at 650 nm emission. This component becomes dominant (59% yield) and longer (2–3 ns) at 700 nm, the observed emission peak of the exciplex. We assign this component to decay from intrachain excitons in M3EH-PPV formed by thermally excited exciplexes, as observed in PFB/F8BT and TFB/F8BT blends.²⁵ In devices, this would result in increased probability of charge separation since the exciplex would act as an exciton scavenger bound to the interface, and its subsequent release of that stored energy provides a second chance for charge dissociation. This decay could also represent a shortened decay directly from the exciplex due to loss to the triplet state, as conjectured in a similar system.²⁸

The reasoning for this assignment is as follows. We see evidence for exciplex emission in the steady-state photoluminescence, and so we expect to see decay from this state in the time-resolved data. Decay directly from the exciplex itself would be represented by a much longer lifetime

(~50 ns) as previously reported.^{26,27,34} Time-resolved decay of pristine M3EH-PPV, however, shows decay of 0.80 ns under certain conditions (low emission energies in nonaggregated samples), suggesting that this component is intrinsic to the M3EH-PPV decay. Additionally, examination of the yield of the 0.78 ns component reveals that it is present in the same proportions as would be expected from the unquenched 11 ns decay component of pristine CN-ether-PPV. Thus, the 0.78 ns emission is characteristic of M3EH-PPV, but related to the presence of CN-ether-PPV, which would be expected to transfer most or all of its charge to the exciplex since its radiative and nonradiative decay rates are already very slow. Finally, the yield of the 0.78 ns state, when scaled by the steady-state photoluminescence yield of the polymers, is largest in the 50 wt % blends and equal to exactly half of the yields of the pristine polymers, as would be expected for an exciplex that is gathering charge from each polymer. This is consistent with the exciplex state decaying by nonradiative recombination to thermally excite the M3EH-PPV exciton.

Both CN-ether-PPV and M3EH-PPV components are easily quenched in most heterojunctions, although CN-ether-PPV decay components are present in blends with 80–86 wt % CN-ether-PPV, as well as in some layered devices, suggesting that a minimum (~25 wt %) fraction of M3EH-PPV is required to completely quench CN-ether-PPV.

The decay of the 30 nm/30 nm M3EH-PPV/CN-ether-PPV layer is strikingly similar (as is the steady-state photoluminescence) to the 86 wt % blend, and contains the decay components of pristine CN-ether-PPV. This was not the case for all layered devices, and the high variability indicates the difficulty of controlling the morphology at the layered interface. A working layered photovoltaic with particularly good device performance exhibited decay components similar to those of a blended device with similarly high performance. Nonoptimized planar layers are either similarly ineffective as a low M3EH-PPV ratio at quenching the excitons in CN-ether-PPV or the layer is partially blended at the interface. CN-ether-PPV chains at this interface are unlikely to be quenched if the polymer chain does not lie flat along the interface. The decay components of M3EH-PPV, however, are efficiently quenched in this planar layer, probably by the same mechanism creating low luminescence in the pristine M3EH-PPV polymer, namely, efficient energy transfer that allows charges to visit quenching sites, either intrinsic or external.

In summary, layers achieve higher power efficiency than neat films by a substantially different mechanism than do blends. The excited-state kinetics of layers and 50 wt % blends varies dramatically despite similarities in *J-V* curves, and the decay of layers approximates that of a 86 wt % blend despite the superior current of layered devices. However, because the PEDOT||Al device geometry results in the M3EH-PPV absorbing an appreciable amount of the photons before the CN-ether-PPV, a much larger fraction of excitons are expected to be generated in M3EH-PPV compared to CN-ether-PPV; therefore, the layers could also achieve more efficient charge collection of exciton dissociated in the M3EH-PPV layers due to the ability to make much thinner layers (i.e., 25 nm) without shorting. The highest short-circuit cur-

rents for layers consisted of very thin M3EH-PPV films (25 nm) and relatively thick CN-ether-PPV films (50 nm) implying that both effects may contribute. To gain further insight into what mechanism is responsible for the increased power efficiency in layers versus neat films we conducted numerical simulations as described below.

B. Modeling J - V characteristics of bilayer devices

We developed a model to simulate both exciton generation rate as a function of position and current-voltage curves for bilayer devices. We used a one-dimensional numerical model to describe absorption of incident light, charge generation, and charge transport within the bilayer device. The model allowed us to calculate current-voltage characteristics for several device thicknesses and architectures where we assume a sharp interface between the donor and acceptor layers and between the electrodes and the organic material. The effect of blending as well as more detailed predictions of our model is considered elsewhere²⁴ and we refer the interested reader to that publication for details.

1. Simulation methods

The absorption as a function of the position within the device can be modeled by solving Maxwell's equations at the layer interfaces with the appropriate boundary conditions. The donor-acceptor structure is sandwiched directly between the PEDOT anode and the aluminum cathode. The propagation and absorption of light is computed by using a transfer-matrix method.³⁵

The absorption is taken to be related to the exciton creation flux J_{exc} (bound electron-hole pairs) by

$$J_{\text{exc}}(\nu, x) = P_{\text{diss}}(\nu, x)/h\nu,$$

where P_{diss} is the dissipated power. Integration over all frequencies ν yields the total exciton creation flux as a function of position x .

Due to the large exciton binding energy in organic materials, exciton dissociation at small electric fields was found to take place predominantly at interfaces of materials with differing chemical potentials/molecular-orbital energies.³⁶ Therefore we only take excitons into account that are created within the exciton diffusion length of either the donor-acceptor interface or the interfaces with the electrodes.

The simulation of the transport is based on a numerical model proposed earlier for the behavior of space charges in organic light-emitting diodes (OLED).³⁶ In this model transport is governed by a system of partial linear differential equations relating current, charge generation, electric field, recombination, and mobility. For the charge injection from the electrodes a thermionic injection model³⁷ is employed. The boundary condition is given by the difference of the externally applied voltage and the built-in potential, taken to be the difference in work functions of the contacts. The steps in the chemical potential due to the internal layer interfaces are taken into account by a Miller-Abrahams form.³⁶ The simulation performs a forward integration of Poisson's equation to obtain the electric-field distribution. Integrating the continuity equation (advancing in time), the electron and

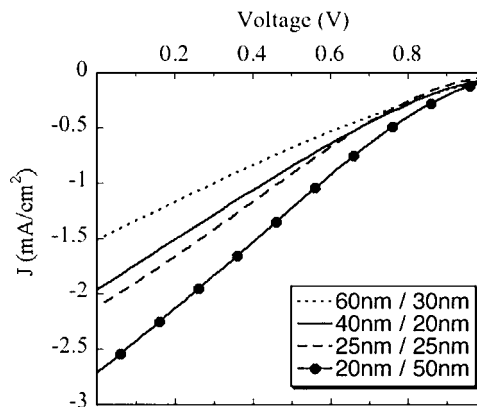


FIG. 7. J - V Curves from experiment of M3EH-PPV/CN-ether-PPV layered devices as a function of layer thickness. The highest current is observed for 20-nm-/50-nm-thick devices. Thicknesses are ± 5 nm. Light intensity is 80 mW/cm^2 solar light.

hole charge densities are increased by the corresponding number of dissociated excitons. The effect of charge trapping is ignored in this simulation.

2. Parameters

The following quantities enter the simulation as parameters. The spectrum and intensity of the incident light, the complex refractive index $n(\lambda)$ of the anode, cathode, donor and acceptor, the work function of the electrodes, the LUMO and HOMO of the organic materials as well as their exciton binding energies and exciton diffusion lengths, the electron and hole mobilities and their field dependence, and the layer thicknesses.

For our simulations, we take the spectrum and intensity (100 mW/cm^2) for the lightbulb used for the experimental J - V measurements, the complex refractive index for Al (Ref. 38) and ITO,³⁹ the absorption (n) and complex index (k) for M3EH-PPV and CN-ether-PPV estimated from absorption and ellipsometry data on CN-PPV (Ref. 40) and MEH-PPV (Ref. 41) taken at IBM and work functions of 5.0 and 4.2 eV for PEDOT and Al, respectively. For M3EH-PPV, we use a HOMO and LUMO level of 5.3 and 3.0 eV, respectively, an exciton binding energy of 0.2 eV, an exciton diffusion length of 20 nm, and a zero-field electron and hole mobility of 10×10^{-6} and $100 \times 10^{-6} \text{ cm}^2/\text{Vs}$, respectively.⁴² For CN-ether-PPV, we use HOMO and LUMO levels of 5.9 and 3.5 eV, respectively, an exciton binding energy of 0.2 eV, an exciton diffusion length of 20 nm, and an electron and hole mobility of 100×10^{-6} and $10 \times 10^{-6} \text{ cm}^2/\text{Vs}$, respectively. The field dependence of the electron mobility and hole mobility is taken as $5 \times 10^{-4} (\text{m/V})^{1/2}$ for both materials. We did not have an independent measurement of the charge mobilities for CN-ether-PPV.

3. Results

The J - V curves from experiment are shown in Fig. 7, and comparison of the short-circuit current for experiment and simulation are shown in Fig. 8. Short-circuit current and fill factors are twice as high in simulation (FF up to 50%) as in experiment (FF $\sim 25\%$), probably due to artificially high mobilities in simulations. The thickness dependence exhibits

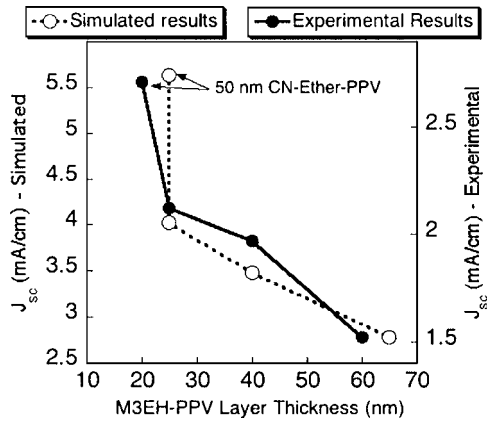


FIG. 8. J_{sc} compared for experimental vs simulated M3EH-PPV/CN-ether-PPV layered devices as a function of M3EH-PPV thickness. CN-ether-PPV is 25 ± 5 nm, except for the points with the highest short-circuit current, in which the CN-ether-PPV thickness was 50 nm. Experimental thicknesses are ± 5 nm. A linear relationship between M3EH-PPV thickness and short-circuit current is observed, except for the 20 nm/50 nm device, in which electric-field maximization due to reflection at the interface results in enhanced current. Open-circuit voltages of 1.2 V are comparable between experiment and simulations.

the same trend in simulation and experiment and is robust across a variety of simulations with different mobilities. In agreement with experiment, numerical simulations indicate that J_{sc} tends to increase as the M3EH-PPV thickness decreases, as expected for transport-limited devices. CN-ether-PPV thickness was inversely proportional to J_{sc} ; charge-transport is therefore not the crucial factor in the thickness of the CN-ether-PPV layer. Out of those layer thicknesses modeled, 25 nm/50 nm M3EH-PPV/CN-ether-PPV gave the best J_{sc} , and 65 nm/25 nm gave the worst. This is roughly paralleled by the experimental data that show similar relative performance for comparable device thicknesses (Figs. 7 and 8).

The simulations further reveal that the clear tail near V_{oc} that gives rise to a relatively large V_{oc} of ~ 1.2 V is due to the buildup of space charge. For layers, when the applied voltage equals the difference in the work functions of PEDOT and Al (~ 0.8 eV), the drift current is zero; however, the diffusion current still remains and is directed towards the contacts because electrons are less likely to jump to the LUMO level of the M3EH-PPV than to randomly diffuse to the Al electrode (and vice versa for holes). Thus, near V_{oc} space-charge effects become more important, and a significant diffusion current resides in the device structure due to the charge-carrier concentration gradient. Similar effects have been observed in simulations of layered films of F8BT/PFB.⁴³ The contribution of diffusion to V_{oc} in blended structures is less significant because a well-defined charge barrier does not exist in the blended device due to the interpenetration of the electron- and hole-transporting species.

To understand why thicker CN-ether-PPV layers result in improved performance, the internal reflection within the device must be considered. With no reflection, exciton generation would attenuate exponentially. Instead, we observe a slight curvature (Fig. 9), resulting from exponential light attenuation combined with absorbed light after reflection at the polymer/polymer and polymer/Al interfaces. We also see evidence for this reflection in experimental quantum effi-

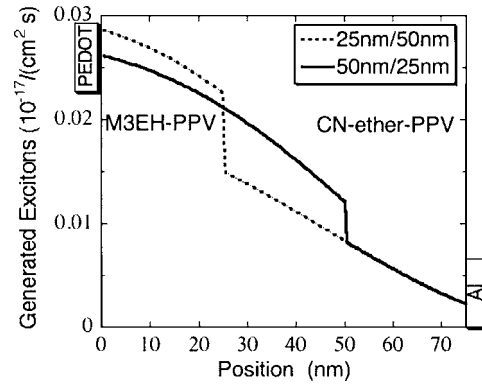


FIG. 9. Exciton generation rate as a function of the two extreme layer thicknesses in layered heterostructured devices measured at 100 mW/cm^2 solar light. Exciton generation can be enhanced in the M3EH-PPV layer due to reflection from CN-ether-PPV/aluminum interface.

ciency measurements, where quantum efficiency is slightly antibatic with the absorption of CN-ether-PPV in some devices. Because of the large amount of light reflection at the CN-ether-PPV/Al interface, the electric field is minimized at that point, reducing exciton generation within the portions of the CN-ether-PPV layer closer to this interface. Thus, the further the polymer/polymer interface is from the CN-ether-PPV/Al electrode, the higher the exciton generation at that polymer/polymer interface and thus the higher the current density until the interference peak is reached (for devices around 100–200 nm thick). Consequently, the superior performance of 20 nm/50 nm layers can be explained by both more efficient charge collection in the very thin M3EH-PPV layer and internal reflection effects, which increases the exciton creation flux density within a diffusion length of the polymer/polymer interface, as seen in Fig. 8. The exciton generation is enhanced by ~ 2.5 times in the 20 nm/50 nm layer over the 50 nm/25 nm layer, and the short-circuit current is enhanced by 1.8 times, indicating that not all additional charge is transported out of the device. Clearly, an optimal set of film thicknesses exists to optimize device efficiency so that the layers are thick enough to maximize absorption and exciton generation (allowing for reflection effects) but thin enough to minimize recombination.

IV. CONCLUSIONS

We have compared blends and layers of hole- and electron-transporting photoconductive polymers in photovoltaic devices. Blended devices tend to outperform layered devices although both show similar optimized photocurrents and efficiencies, and both are characterized by low fill factors due to poor charge transport.

For blended structures, significant exciton quenching occurs in both the electron- and hole-transporting polymers due to the interpenetrating morphology; however, the lack of complete quenching limits the achievable short-circuit currents. In layered structures, decay times were generally longer than for blends and substantial exciton quenching was only consistently observed for the hole-transporting polymer. Thus we conclude that, on average, exciton dissociation and charge transfer are more efficient in blended than in layered

devices. The use of a better electron acceptor would improve the performance of both blended and layered devices, as suggested by recent results⁴⁴ with the electron acceptor BBL (LUMO 4.0 eV), in which MEH-PPV bilayers were similarly quenched in the steady state but time-resolved analysis show an ultrafast decay of 0.012 ns, suggesting highly efficient electron transfer in MEH-PPV/BBL layers.

Both steady-state and time-resolved data indicate that charge transfer occurred to an intermediate exciplex state, which thermally reexcited the M3EH-PPV exciton, providing an additional route for charge separation. This mechanism accounts for high performance of 50 wt % blended devices in which both polymers are present in sufficient volume fraction for charge transfer to the exciplex. Working photovoltaic devices with high currents showed a particularly large exciplex emission in the steady state, and a correspondingly long decay time due to a high yield of the exciplex decay, further supporting the hypothesis that exciplex formation is advantageous to device performance.

Simulations of layered structures reveal that diffusion dominates the device properties when the applied voltage is near the built-in potential, creating space-charge buildup and leading to low fill factors but large V_{oc} 's. Moreover, internal reflection of photons at interfaces strongly affects the exciton generation rate throughout the device so that the best performance is achieved when the polymer/polymer interface is far from the reflective Al electrode. This effect accounts for much of the improved performance in layers, but places limits on the optimal thickness for polymer layers, and poses technical challenges for optimization of this device architecture.

Overall, our results indicate that blended and layered structures achieve improved performance through substantially different mechanisms (namely, exciton dissociation versus exciton generation, respectively) which need to be considered in the device design. In fact, structures that consist of partially blended layers should result in the highest power efficiencies by combining the advantages of both systems. Finally, poor charge mobility, particularly for electrons, substantially reduces the achievable power efficiency in heterostructured polymer photovoltaics.²⁴ Substantial increases in mobility could result in power efficiencies closer to the 5% predicted^{24,45} for M3EH-PPV:CN-ether-PPV blends, with even higher efficiencies for materials with improved absorption across the solar spectrum.

ACKNOWLEDGMENTS

The authors would like to thank Sean Shaheen and the scientists at the National Renewable Energy Laboratories for both useful discussions and use of their equipment for spectroscopic measurements. The authors also thank Alison Breeze and Melissa Kreger for many useful discussions. One of the authors (S.A.C.) acknowledges support from the Beyond the Horizons program of DOE-NREL, Contract No. ACQ-1-306-19-03, for this work. Another author (J.O.H.) acknowledges support from NSF-ECS-0101794. Another author (S.V.C.) acknowledges support from the Graduate Assistance in Areas of National Need (GAANN) scholarship.

- ¹J. J. Dittmer, K. Petritsch, E. A. Marseglia, R. H. Friend, H. Rost, and A. B. Holmes, *Synth. Met.* **102**, 879 (1999).
- ²G. Yu, J. Gao, J. C. Hummelen, F. Wudl, and A. J. Heeger, *Science* **270**, 1789 (1995).
- ³A. C. Arango, P. J. Brock, and S. A. Carter, *Appl. Phys. Lett.* **74**, 1698 (1999).
- ⁴G. Yu and A. J. Heeger, *J. Appl. Phys.* **78**, 4510 (1995).
- ⁵J. J. M. Halls, C. A. Walsh, N. C. Greenham, E. A. Marseglia, R. H. Friend, S. C. Moratti, and A. B. Holmes, *Nature (London)* **376**, 498 (1995).
- ⁶S. A. Jenekhe and S. Yi, *Appl. Phys. Lett.* **77**, 2635 (2000).
- ⁷M. Granstrom, K. Petritsch, A. C. Arias, A. Lux, M. R. Andersson, and R. H. Friend, *Nature (London)* **395**, 257 (1998).
- ⁸K. Tada, M. Onoda, H. Nakayama, and K. Yoshino, *Synth. Met.* **102**, 982 (1999).
- ⁹J. J. M. Halls, K. Pichler, R. H. Friend, S. C. Moratti, and A. B. Holmes, *Appl. Phys. Lett.* **68**, 3120 (1996).
- ¹⁰F. L. Zhang, M. Johansson, M. R. Andersson, J. C. Hummelen, and O. Ingands, *Synth. Met.* **137**, 1401 (2003).
- ¹¹A. J. Breeze, A. Salomon, D. S. Ginley, B. A. Gregg, H. Tillmann, and H.-H. Hoerhold, *Appl. Phys. Lett.* **81**, 3085 (2002).
- ¹²J. A. Osaheni, S. A. Jenekhe, and J. Perlestein, *Appl. Phys. Lett.* **64**, 3112 (1994).
- ¹³K. Feldrapp, W. Brutting, M. Schwoerer, M. Brettreich, and A. Hirsch, *Synth. Met.* **101**, 156 (1999).
- ¹⁴H. Tillmann and H.-H. Hoerhold, *Synth. Met.* **101**, 138 (1999).
- ¹⁵S. Pfeiffer and H.-H. Hoerhold, *Macromol. Chem. Phys.* **200**, 1870 (1999).
- ¹⁶S. C. Veenstra *et al.*, *Chem. Mater.* **16**, 2503 (2004).
- ¹⁷J. Loos *et al.*, *J. Appl. Polym. Sci.* **97**, 1001 (2005).
- ¹⁸P. A. C. Quist, T. J. Savenije, M. M. Koetse, S. C. Veenstra, J. M. Kroon, and L. D. A. Siebbeles, *Adv. Funct. Mater.* **15**, 469 (2005).
- ¹⁹A. J. Breeze, Z. Schlesinger, P. J. Brock, and S. A. Carter, *Phys. Rev. B* **64**, 125205 (2001).
- ²⁰A. C. Arango, L. R. Johnson, V. N. Bliznyuk, Z. Schlesinger, S. A. Carter, and H.-H. Hoerhold, *Adv. Mater. (Weinheim, Ger.)* **12**, 1689 (2000).
- ²¹S. A. Carter, M. Angelopoulos, S. Karg, P. J. Brock, and J. C. Scott, *Appl. Phys. Lett.* **70**, 2067 (1997).
- ²²A. C. Arias, M. Granstrom, K. Petritsch, and R. H. Friend, *Synth. Met.* **102**, 953 (1999).
- ²³D. V. O'Connor and D. Phillips, *Time-Correlated Single Photon Counting* (Academic, London, 1984).
- ²⁴J. O. Haerter, S. V. Chasteen, S. A. Carter, and J. C. Scott, *Appl. Phys. Lett.* **86**, 164101 (2005).
- ²⁵M. M. Alam and S. A. Jenekhe, *J. Phys. Chem. B* **105**, 2479 (2001).
- ²⁶J. A. Osaheni and S. A. Jenekhe, *Macromolecules* **27**, 739 (1994).
- ²⁷A. C. Morteani, P. Sreearunothai, L. M. Herz, R. H. Friend, and C. Silva, *Phys. Rev. Lett.* **92**, 247402 (2004).
- ²⁸T. Offermans, P. A. van Hal, S. C. J. Meskers, M. M. Koetse, and R. A. J. Janssen, *Phys. Rev. B* **72**, 045213 (2005).
- ²⁹L. Smilowitz, A. Hays, A. J. Heeger, G. Wang, and J. E. Bowers, *J. Chem. Phys.* **98**, 6504 (1993).
- ³⁰J. R. Lakowicz, *Principles of Fluorescence Spectroscopy*, 2nd ed. (Kluwer, New York/Plenum, New York, 1999).
- ³¹I. D. W. Samuel, G. Rumbles, C. J. Collison, R. H. Friend, S. C. Moratti, and A. B. Holmes, *Synth. Met.* **84**, 497 (1997).
- ³²I. D. W. Samuel, B. Crystall, G. Rumbles, P. L. Burn, A. B. Holmes, and R. H. Friend, *Chem. Phys. Lett.* **213**, 472 (1993).
- ³³G. Rumbles *et al.*, *Synth. Met.* **101**, 158 (1999).
- ³⁴X. Zhang *et al.*, *Macromolecules* **35**, 382 (2002).
- ³⁵L. A. A. Pettersson *et al.*, *J. Appl. Phys.* **86**, 487 (1999).
- ³⁶B. Ruhstaller *et al.*, *J. Appl. Phys.* **89**, 8 (2001).
- ³⁷J. C. Scott and G. G. Malliaras, *Chem. Phys. Lett.* **299**, 115 (1999).
- ³⁸J. H. Weaver, in *CRC Handbook of Chemistry and Physics*, 63rd ed., edited by R. C. Weast (CRC, Boca Raton, FL, 1984), p. E-363.
- ³⁹R. A. Synowicki, *Thin Solid Films* **313**, 394 (1998).
- ⁴⁰N. C. Greenham, Ph.D. thesis, University of Cambridge, 1995.
- ⁴¹M. Tammer and A. P. Monkman, *Adv. Mater. (Weinheim, Ger.)* **14**, 210 (2002).
- ⁴²L. Bozano *et al.*, *Appl. Phys. Lett.* **74**, 1132 (1999).
- ⁴³J. A. Barker *et al.*, *Phys. Rev. B* **67**, 075205-1 (2003).
- ⁴⁴M. M. Alam and S. A. Jenekhe, *Chem. Mater.* **16**, 4647 (2004).
- ⁴⁵R. S. Echols and C. E. France, *Mater. Res. Soc. Symp. Proc.* **822**, S7.7.1 (2004).